INSTITUTE OF PHYSICS PUBLISHING JOURNAL OF MICROMECHANICS AND MICROENGINEERING

J. Micromech. Microeng. **12** (2002) N7–N17 PII: S0960-1317(02)28844-0

Hybrid macro–micro fluidics system for a chip-based biosensor

C R Tamanaha[1], L J Whitman[2] and R J Colton[2]

[1] Geo-Centers, Inc., PO Box 441340, Fort Washington, MD 20749, USA
[2] Naval Research Laboratory, 4555 Overlook Avenue, SW, Washington, DC 20375, USA

E-mail: cy.tamanaha@nrl.navy.mil

Received 17 September 2001, in final form 9 January 2002
Published 18 February 2002
Online at stacks.iop.org/JMM/12/N7

Abstract

We describe the engineering of a hybrid fluidics platform for a chip-based biosensor system that combines high-performance microfluidics components with powerful, yet compact, millimeter-scale pump and valve actuators. The microfluidics system includes channels, valveless diffuser-based pumps, and pinch-valves that are cast into a poly(dimethylsiloxane) (PDMS) membrane and packaged along with the sensor chip into a palm-sized plastic cartridge. The microfluidics are driven by pump and valve actuators contained in an external unit (with a volume $\sim$30 cm^3) that interfaces kinematically with the PDMS microelements on the cartridge. The pump actuator is a simple-lever, flexure-hinge displacement amplifier that increases the motion of a piezoelectric stack. The valve actuators are an array of cantilevers operated by shape memory alloy wires. All components can be fabricated without the need for complex lithography or micromachining, and can be used with fluids containing micron-sized particulates. Prototypes have been modeled and tested to ensure the delivery of microliter volumes of fluid and the even dispersion of reagents over the chip sensing elements. With this hybrid approach to the fluidics system, the biochemical assay benefits from the many advantages of microfluidics yet we avoid the complexity and unknown reliability of immature microactuator technologies.

1. Introduction

Rapid progress is being made in the development of micro-total analysis systems (μTAS), where complete chemical syntheses or analyses can be performed in a highly compact instrument. The small sample and reagent volumes (typically $<$1 ml) combined with the narrow channel sizes (typically $<$1 mm) in such instruments offer the potential for greatly improved speed and sensitivity compared with more conventional analytical systems. The viability of μTAS depends in part on the development of sophisticated yet robust miniature fluidics components—pumps, valves, mixers, filters, etc—that can be integrated with the analytical sensor and actuator components [1].

Microfluidic components have been fabricated primarily from silicon, glass, and plastic using conventional lithographic techniques. A variety of intriguing microcomponents have been developed to control the movement of fluids, including elements based on acoustic, centrifugal and electromagnetic forces; electroosmotic and electrophoretic effects; micromechanical and pneumatically powered components; and vapor bubbles [1–13]. One of the most promising approaches to developing microfluidics components is the use of printing and molding techniques applied to soft polymeric materials, particularly poly(dimethylsiloxane) (PDMS) [14, 15]. The chief advantage of this approach is the potentially low fabrication cost, which is an important factor for widespread adoption of any technology. However, relatively few integrated systems have come to market yet because of the difficulties in making such components reliable, for example, by avoiding clogging of the microchannels by particles or precipitates.

Report Documentation Page

Form Approved
OMB No. 0704-0188

1. REPORT DATE	2. REPORT TYPE	3. DATES COVERED
JAN 2002		**00-00-2002 to 00-00-2002**

4. TITLE AND SUBTITLE	5a. CONTRACT NUMBER
Hybrid macro-micro fluidics system for a chip-based biosensor	5b. GRANT NUMBER
	5c. PROGRAM ELEMENT NUMBER
6. AUTHOR(S)	5d. PROJECT NUMBER
	5e. TASK NUMBER
	5f. WORK UNIT NUMBER
7. PERFORMING ORGANIZATION NAME(S) AND ADDRESS(ES) **Naval Research Laboratory,4555 Overlook Avenue SW,Washington,DC,20375**	8. PERFORMING ORGANIZATION REPORT NUMBER
9. SPONSORING/MONITORING AGENCY NAME(S) AND ADDRESS(ES)	10. SPONSOR/MONITOR'S ACRONYM(S)
	11. SPONSOR/MONITOR'S REPORT NUMBER(S)

12. DISTRIBUTION/AVAILABILITY STATEMENT
Approved for public release; distribution unlimited

13. SUPPLEMENTARY NOTES

14. ABSTRACT

We describe the engineering of a hybrid fluidics platform for a chip-based biosensor system that combines high-performance microfluidics components with powerful, yet compact, millimeter-scale pump and valve actuators. The microfluidics system includes channels, valveless diffuser-based pumps, and pinch-valves that are cast into a poly(dimethylsiloxane) (PDMS) membrane and packaged along with the sensor chip into a palm-sized plastic cartridge. The microfluidics are driven by pump and valve actuators contained in an external unit (with a volume ~30 cm3) that interfaces kinematically with the PDMS microelements on the cartridge. The pump actuator is a simple-lever, flexure-hinge displacement amplifier that increases the motion of a piezoelectric stack. The valve actuators are an array of cantilevers operated by shape memory alloy wires. All components can be fabricated without the need for complex lithography or micromachining, and can be used with fluids containing micron-sized particulates. Prototypes have been modeled and tested to ensure the delivery of microliter volumes of fluid and the even dispersion of reagents over the chip sensing elements. With this hybrid approach to the fluidics system, the biochemical assay benefits from the many advantages of microfluidics yet we avoid the complexity and unknown reliability of immature microactuator technologies.

15. SUBJECT TERMS

16. SECURITY CLASSIFICATION OF:			17. LIMITATION OF ABSTRACT	18. NUMBER OF PAGES	19a. NAME OF RESPONSIBLE PERSON
a. REPORT	b. ABSTRACT	c. THIS PAGE			
unclassified	**unclassified**	**unclassified**	**Same as Report (SAR)**	**11**	

We are developing a μTAS, the bead array counter (BARC), for multiplex detection of specific nucleic acid sequences [16]. Conceptually, the BARC biosensor is similar to a 'gene chip', which simultaneously looks for a large number of distinct segments of deoxyribonucleic acid (DNA). This is accomplished using an array of DNA spots ('probes') immobilized on a surface (the 'chip'), with each spot containing single strands of one particular segment of interest. When the complementary strands are present in a sample, they hybridize on the chip. In most gene chips, the resulting double-stranded DNA molecules are labeled with fluorescent molecules, and the chip is 'read' with an elaborate imaging system. In the BARC biosensor, the fluorescent labels are replaced by magnetic labels that can be *individually* detected using an array of magnetic field microsensors in the chip. The magnetic labels are commercial magnetic beads 1–3 μm in diameter. The sensors are μm-scale wire-like structures made with giant magnetoresistive (GMR) material. When a magnetic bead is present above a GMR sensor, the resistance decreases by a detectable amount; the more beads present, the larger the decrease. Hence, the BARC approach replaces the optical system required for fluorescence-based detection with simpler and more sensitive and compact microelectronics.

The BARC biosensor system has been initially developed for the detection of biological warfare agents, with the goal of producing a fieldable prototype within the next few years. Although proof-of-concept demonstrations have been performed using external fluidics (via syringe manipulation or manual control of a peristaltic pump), the prototype will require an integrated fluidics system. An ideal approach would use low-cost, disposable cartridges containing all required reagents and have the fluidics fully automated. There are several fluidics requirements to achieve this ideal, some of which are peculiar to BARC. The principle requirement is to automate the flow of microliters of sample and reagent fluids across the sensor chip surface. Moreover, the fluids must be evenly dispersed across the sensor chip so that all elements in the sensor array are uniformly addressed. In addition, the magnetic nature of the assay requires that all materials be fabricated from nonmagnetic components. Another complication is the integral use of micron-scale particles, which requires that all components be resistant to clogging. Other objectives include easy fabrication, compatibility of the fluidics materials with the assay biochemistry, and minimal carryover contamination between assays.

In this paper, we describe the engineering of an integrated fluidics system for the BARC μTAS biosensor system. In order to meet the specific requirements of our application, maintain a reasonable prospect for completion of a fieldable system in the near term, and achieve the goal of reduced cartridge expense, we have developed a hybrid macro–micro fluidics platform (figure 1). In particular, the more complex pumping and valving system is constructed of robust 'macro' components, permanently integrated in a table-top readout instrument package, which interface kinematically with PDMS microelements on a separate cartridge to achieve fluidic control.

2. Design and fabrication of the fluidics system

The fluidics system consists of four discrete components: (1) a flow cell, which is mounted on top of the sensor chip;

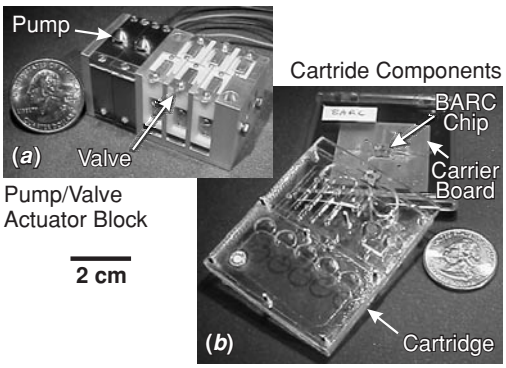

Figure 1. Photographs of (*a*) the pump and valve actuator block, and (*b*) a prototype fluidics cartridge resting on a display box containing the sensor chip mounted on a printed circuit carrier board. Note that this cartridge prototype, designed for testing and evaluation of the fluidics actuators, does not include a mount for the carrier board.

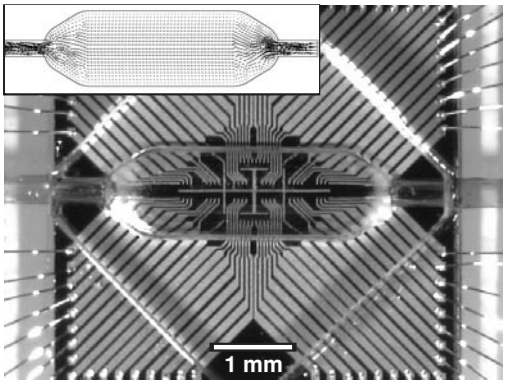

Figure 2. Top view of the quartz flow cell mounted on a BARC sensor chip. The inset shows the results of a fluid flow model used in the design of the cell.

(2) a PDMS membrane into which pump and valve membranes and fluid reservoirs have been molded; (3) the plastic fluidics cartridge, which houses the sensor chip and fluidics; and (4) the pump and valve actuator system, collectively called the actuator block. With the exception of the flow cell, all components can be constructed using simple techniques and equipment.

2.1. Quartz flow cell

The uniformity of the analyte dispersion across the GMR sensors was assessed with fluid flow models. Uniformity is critical for assay-to-assay consistency because if a certain sensor were, for example, to receive significantly more beads than another, it would register a false positive or negative. The problem is compounded by the disparity between the exit diameter of the inlet tube from the microfluidic network (300 μm) and the width of the sensor array (740 μm). Numerical finite-element analysis (FEA) simulations based on ANSYS/FLOTRAN^{TM} indicated that the simplest effective channel geometry is one in which a narrow inlet channel gradually expands from the inlet tube to the wider cross-sectional area of the flow cell. Under laminar flow conditions, this creates a velocity profile that is symmetric along the central flow axis with a weakly parabolic leading edge. This feature has been incorporated in the design of the prototype flow cell (figure 2) [17].

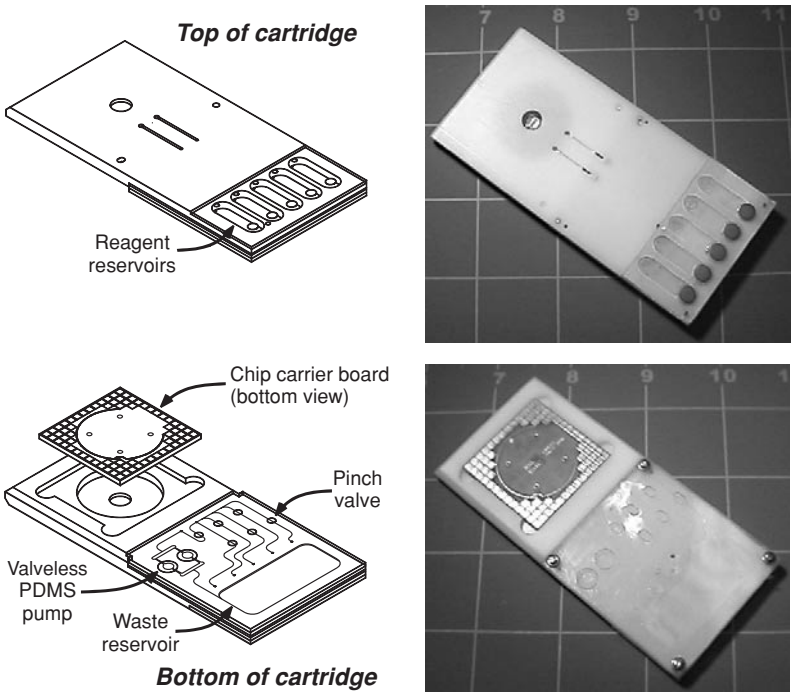

Figure 3. Schematic and photographs of a fully assembled fluidics cartridge. The grid visible in the photographs is in inches.

Initial prototype flow cells, with an internal volume of 1.5 μl, were made from quartz by high precision mechanical diamond tool machining (Mindrum Precision, Inc., Rancho Cucamonga, CA). With quartz, we gained the benefit of reusability and simple attachment of the cells to the BARC chip using UV curing epoxy (Norland optical adhesive No 72; Norland Products, Inc., New Brunswick, NJ). Two, 4 mm long 28-gauge (0.305 mm ID, 0.356 mm OD) polyimide tubes are press-fit into the inlet and outlet grooves of the cell. These tubes connect to standard microbore Tygon® tubing (0.254 mm ID, 0.762 mm OD) that lead to the rest of the fluidics system.

Attachment of the cell to the BARC chip occurs after DNA probes have been arrayed over the GMR sensors. This step is performed on an optical breadboard under an inspection microscope using an XYZ micromanipulator fitted with vacuum tweezer and compression post attachments. These tools are used to align and maintain the position of the quartz cell on the BARC chip during application and curing of the UV epoxy. We have found that despite the 1 μm-high electrical traces on the chip, the epoxy is sufficiently viscous to wick between the cell, polyimide tubing connectors, and chip surface without entering the fluidics chamber that encloses the GMR sensors. In addition, the epoxy does not affect the flow of microbeads at the peripheral interface of the fluidics chamber. The epoxy is allowed to cure under a 366 nm UV lamp for a minimum of 1 h to assure complete polymerization and a watertight seal. Since the quartz cell attachment is done after DNA probe arraying of the chip, the UV lamp wavelength was chosen to prevent photochemical DNA modification, which can occur between 290 and 320 nm [18, 19]. Time-dependent tests from 10 min to 2 h using this lamp on DNA-spotted surfaces have shown no deleterious effects on assays performed on these samples.

2.2. Fluidics membrane and prototype cartridge

As part of the integrated sensor and fluidics system, we have developed a cartridge that includes the BARC chip mounted on a printed circuit carrier board (figure 3) and a poly(dimethylsiloxane) (PDMS) fluidics membrane. Micron-scale channels, negative displacement pumps, membrane valves, and a fluid reservoir are all molded in a single step into a 1 mm thick planar PDMS membrane.

PDMS (Dow Corning SYLGARD® 184 Silicone Elastomer) exhibits properties that make it ideal for rapid production of microfluidic components. Characteristics such as bio- and chemical compatibility, mechanical robustness, and cheap fabrication processes has made it popular for use in gaskets and septa [20], micro-contact printing [21], microfluidic networks for surface patterning of proteins [22], disposable DNA analysis devices [14], and single embryo culture [23]. Applied as a pump diaphragm, the flexible silicone membrane, which exhibits relatively low Young's moduli and high Poisson's ratio [24], allows a large stroke volume with respect to the dead volume of the pump chamber. Increased fluid displacement at comparable excitation frequencies is evident in comparison to more traditional membranes made of, for example, brass, silicon, or Pyrex glass [5, 25].

The primary active component of the fluidic membrane is the dual-chamber PDMS pump, based on the valveless diffuser/nozzle pump first introduced by Stemme and Stemme [26]. This remarkably elegant pump design, whose functionality relies on tapered microchannels in the form of a diffuser/nozzle to create fluidic rectification, is well suited to the low cost, low profile, and rapid construction needs of our cartridge. In general, the nozzle/diffuser acts to decelerate or accelerate fluid flow (depending on flow direction) as fluid traverses along its changing cross-sectional area. The volume

flow for a given pressure drop is greater in the diffuser direction than in the nozzle direction. This results in the net flow of fluid from the inlet to the outlet of the pump. In addition, since there are no moving parts—specifically check-valves—wear, fatigue and obstruction or damage by particulate matter such as magnetic microbeads is minimized. Our PDMS pump has two 3.175 mm diameter chambers. Inlet width, outlet width, and length of the four diffusers are 100 μm, 560 μm, and 3.78 mm respectively. Given these dimensions, the volume of each pump chamber is approximately 1 μl, and approximately 5 μl for the entire pumping unit.

In order to produce these fluidic components in PDMS, a master with patterns of positive relief brass was fabricated. The master was constructed by the standard printed circuit board (PCB) fabrication technique of chemical etching. First, the pump and channel patterns were created in AutoCAD® on a computer. The mask image was then reproduced on a special transfer paper (Toner Transfer System, DynaArt Designs) by feeding it through a standard laser printer at the darkest printer setting. Special care was taken to assure that the transfer paper was properly hydrated by briefly suspending it over a container of heated water prior to feeding it through the printer. This promotes defect-free transfer of toner to the paper.

The transfer paper manufacturer's basic recommended procedures for chemical etching were followed [27], with only minor modifications. Instead of a copper clad PC board, an appropriately sized 50.8 mm × 50.8 mm × 0.125 mm thick brass sheet was used. The transfer sheet was aligned over the brass sheet with the toner mask pattern facing the brass. The stack was placed transfer sheet down on a hot plate set at ∼300 °C. Once the mask had been transferred to the brass sheet, any imperfections in the mask was filled in with etch resist ink. The brass sheet was attached to a glass plate with adhesive (3M Super 77). Then exposed areas of the brass sheet was etched away within 20 min using standard $FeCl_3$ PCB etchant solution that was constantly recirculated over the masked brass surface. This procedure resulted in a network of fine brass lines that made up the channels, pumps, valves, and reservoirs of the master. The toner mask was removed with acetone, and any slivers of brass still attached to the mold were cut away. To complete the master, a 1 mm thick polycarbonate frame with an inside dimension of 49 mm × 55 mm (to contain the pre-polymer solution) was centered around the brass features and secured to the glass base with adhesive (figure 4).

Because of the relatively thick brass sheet that was used, the extra time needed to perform the chemical etch resulted in a gradual breakdown of the toner mask, exposing some of the underlying brass to the etchant. To prevent excessive pitting of the brass, the etch needed to be terminated prematurely, causing the channels to have a trapezoidal-like cross-sectional shape (approximately 125 μm wide on top, tapering to 250 μm at the base). The channels were approximately 125 μm deep. Although the walls of the PDMS channels made by this method were not perfectly smooth in comparison to one from a master made by traditional micromachining techniques (e.g. LIGA, DRIE) [25, 28], its effects on fluid flow under laminar conditions should be insignificant.

To cast the PDMS, a mixture of pre-polymer, either 10:1 or 5:1 weight ratio of base to curing agent, weighing 3.85 g or 3.68 g, respectively, was thoroughly mixed then degassed in a desiccator under vacuum for 30 min. The mixture was poured into the mold and allowed to stand for 5 min to self-level. The PDMS fluidics membrane was cured by either placing the mold on a hot plate set at 65 °C for 4 h, or by putting it in an oven set at 80 °C for 1.5 h. Once cured, the fluidics membrane was carefully peeled from the master.

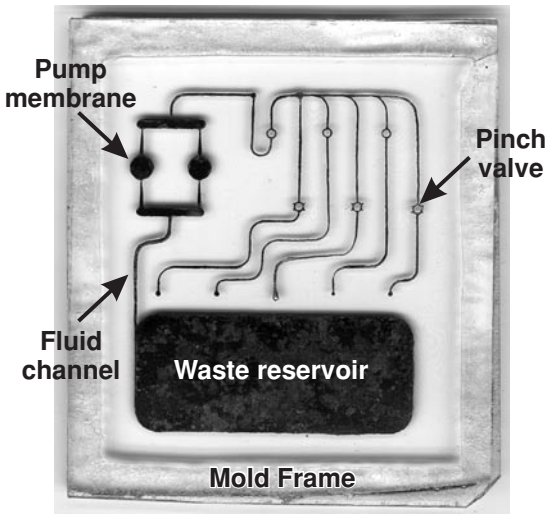

Figure 4. Photograph of the positive relief brass mold used to create the fluidic channels, pump membranes, and pinch valve membranes from PDMS.

There are two seemingly unrelated issues that must be considered when attaching the fluidics membrane to the cartridge: its overall robustness during routine handling and the natural hydrophobic nature of PDMS. Since the cartridges must be robust when handled, we cannot rely solely on the reversible hermetic seal formed by spontaneous adhesion that is characteristic of PDMS to various materials. To seal the fluidic membrane, and thereby form enclosed channels, the PDMS membrane is secured to the cartridge with a sheet of medical grade double-sided tape (Adhesives Research, ARcare 7841). Holes are punched out of the adhesive sheet at locations corresponding to the channel inlets of the PDMS membrane. There are several advantages to using this adhesive tape. Because the tape was designed to promote the lateral flow of fluid in capillary-based diagnostic devices, it was not necessary to oxidize the PDMS surfaces [14] to make them hydrophilic for our application. Therefore, the fluidics membrane can be used directly from the mold. In addition, the seal with the adhesive tape is reversible, so if carefully separated from the cartridge, the PDMS membrane is robust enough to be cleaned and reused if desired.

As already mentioned, unmodified PDMS surfaces tend to be hydrophobic. This property can present undesirable conditions such as priming difficulties, and the formation of bubbles that can prevent the formation of a pressure gradient across the diffuser/nozzle elements rendering the pump useless. The medical grade tape used to adhere the PDMS membrane to the cartridge satisfactorily helps to alleviate many of these problems. However, one of the built-in benefits of the DNA assay buffer solution to be transported by the fluidics system is the inclusion of detergent which decidedly circumvents all of these issues. Depending on the

assay, the buffer solution calls for either 0.0125% w/v or 0.125% w/v of the detergent sodium dodecyl sulfate (SDS). The addition of detergent tends to lower the surface tension of the fluid causing the collapse of existing large bubbles into finer ones during fluid compression in the pumping chamber by the high forces imparted by the pump actuators. These very fine bubbles are quickly purged from the pumps.

Contact angle measurements comparing water with the two SDS concentrations of buffer solutions on PDMS and adhesive tape were made. The results indicate that for both surfaces hydrophilicity is significantly increased with the addition of detergent. In addition, the contact angles, and thus the surface energies, of both materials become comparable at the highest SDS concentration ($75.5^\circ \pm 1.02^\circ$ for 0.125% SDS on PDMS; $73.7^\circ \pm 1.6^\circ$ for 0.125% SDS on ARcare 7841 tape). These results demonstrate that further PDMS surface treatment is unnecessary. All tests described below were performed on membranes secured to a solid substrate in this fashion. It should be pointed out, however, that if a permanent seal is required, one need only raise the surface energy of the PDMS by exposing it to a plasma source (e.g. corona discharge from a handheld Tesla coil or oxygen plasma treatment). This process causes a permanent attachment between the PDMS and the adhesive sheet, such that attempts at removal destroy the PDMS membrane.

A completed cartridge assembly is shown in figure 3. The 10.2 cm × 5.1 cm × 0.55 cm body made of machined Delrin has reagent reservoirs and an area to retain the chip carrier board (by press-fit). The PDMS fluidic membrane and a protective 1 mm thick polycarbonate sheet is attached to the underside of the cartridge. Assay reagents are loaded into the five available reservoirs by injection through the individual septa (seen along the end on the topside of the cartridge). Each reservoir holds 100 μl of solution. The reagents pass through holes in the cartridge to corresponding microfluidic channels in the PDMS. Fluid is transported to and from the quartz cell on the BARC chip through microbore Tygon® tubing. The tubing is set flush inside parallel channels on the topside of the cartridge and is connected to the PDMS fluidic channels via 26 gauge hypodermic stainless steel tubing (type 316) connectors that pass through the cartridge to specific points along the fluidic channel network (not shown). The combined volume of the PDMS microfluidic channels and pumps, microbore tubing, and quartz cell is approximately 12 μl of which about 40% (5 μl) of the dead volume is due to the valveless pumps.

2.3. Pump actuator design

Like the original valveless diffuser/nozzle pump on which it is based [26, 28, 29], the dual-chamber PDMS pump is powered by piezoelectric actuators. However, we have separated the pump actuators from the PDMS pumps, uniting them when the cartridge is inserted into an assembly of the BARC box [17]. The pump actuators are components of the 'actuator block', that also include valve actuators, whose entirety fits in a 25.4 mm × 25.4 mm × 50.8 mm volume (figure 1). In addition to coupling the actuator block to the PDMS pumps and valves on the cartridge, this assembly invokes a plunger mechanism that locks the cartridge in place and engages spring-pin electrical contact with 68 connectors on the BARC chip (figure 5).

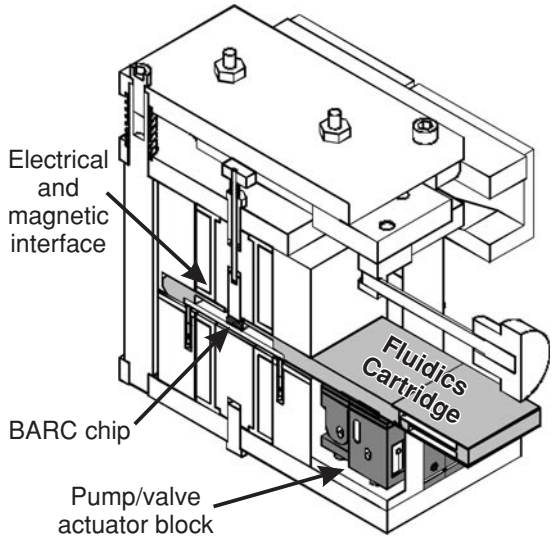

Figure 5. Cutaway cross-sectional view of the complete mechanical assembly—with the cartridge inserted—used when performing an assay. This assembly mechanically couples the cartridge to the electrical interface and the pump/valve actuators within the custom electromagnet needed for sensor chip operation.

There are several design advantages in a modularized cartridge and actuator system. In the original valveless diffuser/nozzle pump in which a PZT disk is permanently mounted to the pump chamber diaphragm, it was determined that mass loading of the pump diaphragm is dominated by the fluid in the diffuser/nozzle elements as a result of large fluid acceleration in the narrow elements [29]. By substituting the PZT disk with piezoelectric stacks that can rapidly generate large forces via a mechanically coupled actuator system, the mass loading effect is removed, and the diaphragm is no longer dominated by the oscillating fluid in the pump. Operationally, there is no need to rely on a natural resonance frequency to generate an optimal pumping rate. The flow rate can therefore be linearly varied by excitation frequency rather than by excitation voltage. In addition, the power consumption of piezoelectric stacks increases linearly with frequency and actuator capacitance, which can generate undesirable heat. Separating the piezoelectric stacks from the PDMS pumps therefore eliminates the transfer of generated heat from the piezos to the solution during high-frequency operations. Finally, because the actuators are removed from the cartridge, the cartridge can be made with a minimal number of inexpensive parts, most being synthetic polymers, thus reducing its overall cost and production time. It then becomes more feasible for these cartridges to be mass produced in quantity and disposed of after a single use.

The use of piezoelectric stacks to actuate a micropump has previously been demonstrated by Shoji *et al* [3]. In this implementation, micropumps capable of non-pulsatile liquid flow and controllable flow rates were integrated on a silicon wafer for use in chemical analyzing systems. One of the disadvantages of this early silicon-based micropump was the need to permanently attach large stacks to the Pyrex glass diaphragm of the pump in order to achieve a

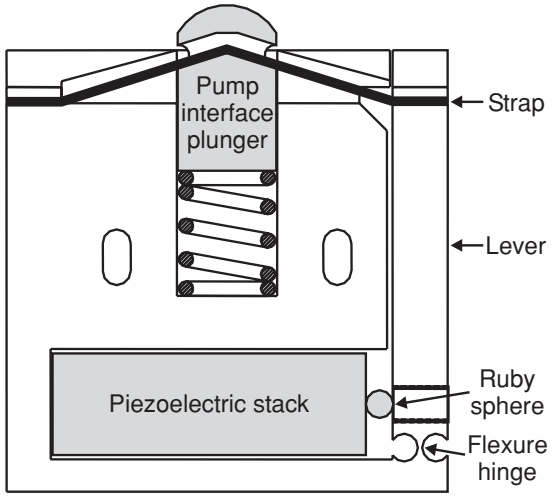

Figure 6. Cross-sectional drawing of the principal components in a pump actuator. The horizontal motion of the piezoelectric stack is transferred by the lever and strap linkage into an amplified vertical motion of the pump interface plunger.

linear displacement sufficient to open the passive one-way polycrystalline silicon valves and expel liquid. Our valveless PDMS pump also requires a nominal diaphragm displacement, not only to eliminate dead space in the chamber during compression, but to obtain a ratio (η) of the pressure loss coefficients of the nozzle (ξ_n) and diffuser (ξ_d), such that $\eta = \xi_n/\xi_d$, is as large as possible [29]. We use a piezoelectric stack coupled to a simple lever (class-3) flexure notch hinge displacement amplifier to provide a minimum of 100-μm diaphragm displacement and fulfill these requirements.

Two compact displacement amplifiers were designed, each 25.4 mm $\times$ 25.4 mm $\times$ 7.94 mm. A schematic representation of one amplifier is shown in (figure 6). Each amplifier is a compact, synergistic mechanism utilizing a lever arm with a monolithic flexure hinge fulcrum, and a flexible beam and plunger linkage. It is devised to precisely magnify the small deformation of a horizontally positioned piezoelectric stack into a large vertical plunger displacement. Upon application of a driving voltage, the length of the piezoelectric stack increases, pushing against the lever arm. The lever was calculated to magnify a 10 μm (nominal) stack motion by 8.12 times. The motion of the lever is amplified an additional 1.54 times by the flexible V-shaped beam that under tension pulls down on the plunger and causes its vertical displacement of 125 μm. Therefore, only 80% of the nominal driving voltage must be applied to the piezo stack to meet the 100 μm pump diaphragm displacement required for satisfactory fluid pumping.

A key feature of the system is the 250 μm thick (at its narrowest point along the spine) monolithic flexure hinge which ensures a smooth, maintenance-free operation with zero-backlash and no stick-slip friction. Material selection was based on characteristics beneficial to a class-3 mechanical amplifier with a flexure-hinge that is expected to undergo rapid oscillation: a high strength-to-weight ratio, and a Young's modulus capable of achieving high amplifier efficiency yet consuming little energy. Titanium (commercial grade, GR4) was chosen because its physical properties were a compromise

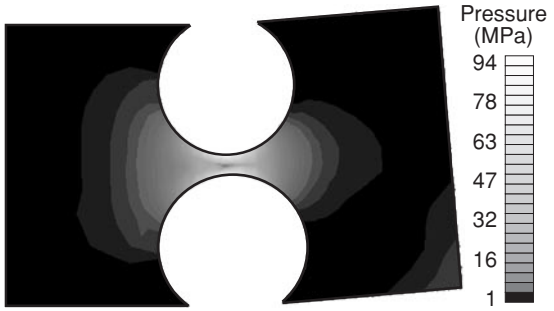

Figure 7. The stress on the flexure notch hinge caused by a force applied to the lower right corner, as calculated with a finite element analysis. Note that a very nonlinear gray scale is used to make the stress gradients more apparent.

between those of lower durability aluminum and higher durability stainless steel. Titanium is nonmagnetic with a tensile strength of 550 MPa that approaches stainless steel but at nearly half the stiffness with a modulus of elasticity of 104 GPa.

Although other structures might have been chosen (e.g. leaf, elliptical, 'corner filleted'), the notch hinge is immune to parasitic forces and has a localized axis of rotation [30, 31]. However, this geometry results in high local stresses that prevent large deflections ($\gtrsim$100 μm). Prior to construction, simulations were performed to verify that the titanium material would withstand the stress incurred by the flexure notch hinge. Because the amplifier arm is relatively thick in comparison to the hinge spine, we can assume that the arm motion will be in a plane normal to the arm thickness with negligible out-of-plane motion. Therefore, two-dimensional, finite element analysis using the solid element named PLANE82 in ANSYS was applied. This 8-node element, with two degrees of freedom at each node, provides results that are more accurate for irregular shapes and for curved boundaries in particular. An anticipated applied displacement of approximately 10 μm made 2.5 mm away from the center thickness of the hinge spine was simulated (figure 7). Results show that the maximum stress at the center thickness of the spine is 94 MPa. This stress is a little more than 1/6th of the ultimate tensile stress for titanium. Therefore, the flexure hinge will remain well within the fatigue limit for the material.

Wire electrodischarge machining (EDM) was used to fabricate the flexure hinge, lever arm, and piezoelectric stack receptacle from a single titanium blank. Motion and energy from the stack is transferred to the lever arm via a 1.59 mm diameter synthetic ruby sphere. This sphere also serves to allow rotational freedom at the lever-piezoelectric stack interface, and prevent damage to the stack by bending and shear forces. The sphere is isolated in the hollow tip of a set screw (located at the point of effort in the lever arm) that is used to pre-load the piezoelectric stack. A titanium plunger with a return spring ($k = 1.22$ N mm^{-1}) inserts in the titanium body. The plunger, which interfaces with the PDMS membrane fluidics, has a contact radius of 3.3 mm. For the 'V-shaped' beam, a 50.8 μm thick, 25.4 mm long stainless-steel strap is fed through the titanium plunger. The straps were produced by the same chemical milling method described above to create the fluidic PDMS membrane master. The length was chosen so

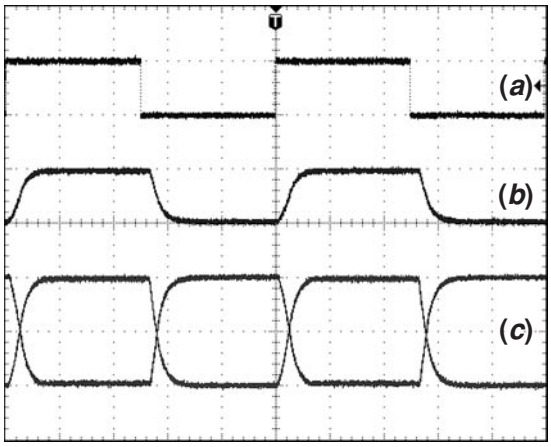

Figure 8. Oscilloscope traces recorded during operation of the piezoelectric stacks in the pump actuators. (*a*) The square-wave output of the function generator (5 V_{p-p}). (*b*) The conditioned signal (500 Hz low-pass filtered). (*c*) The amplified signal applied to the piezoelectric actuator in each pump (100 V_{p-p}, one of which is phase-shifted by 180°).

that when in place, the strap pre-loads the plunger against the return spring. It was calculated that a counter force >2.69 N would then be required to compress the spring beyond the preloaded state and subsequently prevent the actuator from working optimally. One end of the strap is secured to the lever arm and the other to the titanium body. Friction wear at the point of sliding contact between the titanium plunger and strap is reduced by Teflon tape applied to the section of the strap susceptible to damage.

Two independent power amplifiers with a maximum output of 100 V_{p-p} each are used to provide the excitation voltages to the two piezo stacks mounted in the pump actuators. A function generator provides the control signal to the amplifiers. Both sinusoidal and square wave signals have been evaluated; it was determined that square wave excitation provides the most output volume from the pumps (data not shown). The square wave input is conditioned by a low pass filter with an RC time constant ($f_c \approx 500$ Hz) such that the leading and trailing edge of the square wave is rounded off (figure 8). This significantly decreases the 'hammer' effect on the piezos while providing the most efficient fluid displacement from the pumps.

2.4. Valve actuator design

Control of the open/closed states of individual microfluidic channels was achieved using the PDMS material in which the channels are formed. By locally compressing the pliable PDMS material above a channel, fluid flow can be stopped in a manner analogous to a pinch valve. A schematic representation of a valve actuator is shown in figure 9. An array of six valve actuators was constructed. The actuator body, made of Delrin, supports a brass and polycarbonate-composite cantilever beam to which shape memory alloy (SMA) wire is attached. The cantilever was also fortified with spring metal to improve the compressive force on the PDMS valve and maintain a suitable bias force for the SMA wire. The compressive force against the PDMS for this normally

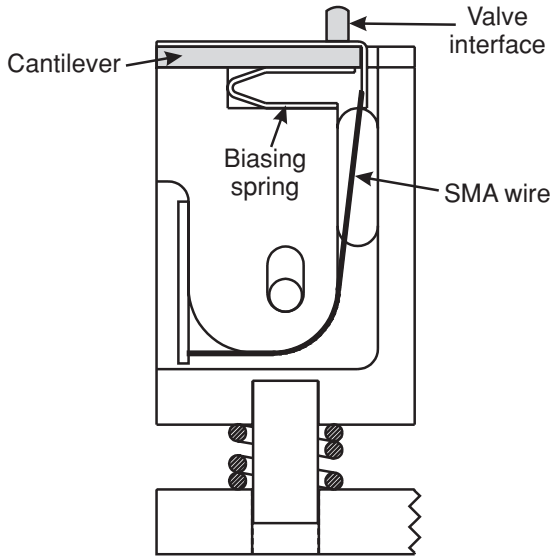

Figure 9. Cross-sectional drawing of the principal components in a valve actuator. The deflection of the cantilever is controlled by the SMA wire. When a current is applied, the wire shrinks in length causing the cantilever to bend downwards. The biasing spring allows the cantilever to return to its starting position once power to the wire is removed.

closed valve is provided by a bead (1.47 mm height, 1.12 mm radius) mounted on each of the cantilever beams. The SMA wire exhibits a cyclic shape memory effect (SME) in which it changes from an austenitic phase (wire contracts) when heated to a martensitic phase (wire relaxes) when cooled. Applying an electrical current to the SMA wire causes it to heat and forces the beam to which the wire is attached to retract from the PDMS, thus reestablishing fluid flow through the channel.

It is recommended that SMA wire only contract 3–5% of its resting length when heated to its activation finish temperature, 78 °C [32]. Therefore, to produce the required cantilever displacement, a sufficient length must be used. To ensure the largest possible cantilever displacement, the Delrin block has been machined with an inner 'mesa' having a bend radius of 3.81 mm to allow a 19 mm length of SMA wire to be wrapped around it. This translates to a contraction, with a constant force, between 0.57 mm and 0.95 mm for the 19-mm long wire. To keep power expenditures low and the cycle rate high, 100-μm diameter SMA wire was used. At this diameter, two SMA wires must be used in parallel to supply enough contraction force. Both ends of the pair of wires were fixed in place under tension to the cantilever and a metal anchor attached to the Delrin body with heat resistant epoxy (Dexter Hysol EA9460). For thermal protection, the surface of the mesa was covered by a thin strip of brass. Although the melting point of Delrin is about 178 °C, above the activation finish temperature of the SMA wire, the brass strip will protect the mesa from deformation in the event excess current is inadvertently applied to the wire. Finally, activation of the SMA wire for each valve actuator is made with a pulse width modulation circuit at an 8.7% duty cycle. The power is directed to each valve actuator through a demultiplexing circuit suitable for computer interfacing and control.

Table 1. Load measurements taken of PDMS membranes at selected compression distances.

Force (N) versus compression distance (μm)			
Base: curing agent	50 μm	150 μm	350 μm
Pump membrane			
5:1	0.059 ± 0.005 N	0.241 ± 0.005 N	1.37 ± 0.01 N
10:1	0.050 ± 0.005 N	0.216 ± 0.005 N	1.32 ± 0.01 N
Bulk membrane			
5:1	0.125 ± 0.005 N	0.767 ± 0.005 N	2.95 ± 0.01 N
10:1	0.099 ± 0.005 N	0.696 ± 0.005 N	2.24 ± 0.01 N

Table 2. Compression forces and distances required to stop fluid flow in PDMS channels.

	Compression force (N) and distance (μm) versus fluid pressure (kPa)		
Base: curing agent	1 kPa	2.36 kPa	-37.92 kPa
5:1	1.54 N, 500 μm	$>$1.54 N, 500 μm	$>$1.67 N, 520 μm
10:1	1.25 N, 500 μm	$>$1.25 N, 500 μm	$>$1.47 N, 550 μm

3. Performance characteristics

3.1. Compression of the PDMS fluidic membranes

The efficiency of the PDMS pumps and valves is predicated on the satisfactory coupling of the actuator block to the fluidic membrane. Of primary interest is the resilience of the PDMS membrane to deformation following compression by the actuators, and the degree of compression that is necessary to establish functioning fluidic components. These factors were taken into consideration when designing the pump and valve actuators.

The compressibility of the PDMS material as a function of the ratio of base to curing agent was examined. Two weight ratios were tested, 10:1 and 5:1. The PDMS mixtures were cured in the brass mold as 1 mm thick membranes (including fluidics) as described above, transferred to glass plates to seal the fluidic channels, and placed on an optical breadboard under the probe of a load cell (Model GSO-1K, Transducer Techniques, Temecula, CA). The load cell was mounted on a three-axis micromanipulator stage with one micromanipulator movement normal to the optical breadboard such that precise compression distances could be easily controlled. To correctly mimic the area of contact between the actuator interface and PDMS surface, the PDMS samples were tested with a probe fitted with a tip that was identical to the titanium plunger interface used in the pump actuators. Two areas of the PDMS fluidics membrane were tested for comparison: the pump diaphragm (875 μm thick) and the bulk membrane (1 mm thick) at a location other than above the fluidic channels or the pump. For each location, load measurements were taken at predetermined compression distances of 50, 150, and 350 μm relative to the uncompressed PDMS surface (table 1).

As expected, the 10:1 ratio PDMS was softer overall than the more polymerized 5:1 ratio. However, the affect of the prepolymer ratio was more apparent at the highest compression distance and on the bulk membrane in particular. The difference between the two bulk membranes was 0.71 N. In contrast, the ratio had a smaller effect on the compression of the pump diaphragm, with a difference of about 0.009 N at the lowest compression and about 0.05 N for the highest measured compression.

The effect of prepolymer ratios on the ability of the valve compression to stop fluid flow was also tested. Like the pump testing strategy, the load cell probe was fitted with a tip identical to the cylindrical bead used on the valve actuators. A section containing only microchannels was cut out from the PDMS fluidic membrane and secured to a glass microscope slide with double-sided transfer tape (ARcare 7841). A hole was punched out at one end of the channel for a well-to-capture fluid and a 26 gauge stainless steel hypodermic tube was inserted into the other end of the channel. A variable height water source was connected to the hypodermic tube with Tygon tubing. Measurements of the load on the valve membrane (875 μm thick) required to impede fluid flow were taken at pressures of 1, 2.36 and -37.92 kPa. The two positive pressure measurements were done by raising the water source to the required heights. The negative pressure measurement was done by applying a vacuum at the output end of the channel while keeping the water source level with the channel. The compression forces and distances required to stop fluid flow are summarized in table 2.

Although pump diaphragm performance is adequate for both polymer ratios, the valve performance is better with a ratio 10:1. In practice, the pressures will be much lower during actual operation of the fluidics. In the assembled cartridges, the maximum height difference between the supply reservoirs on the top layer of the cartridge and the waste reservoir underneath the cartridge is 5 mm, corresponding to a pressure difference of $\sim$50 Pa. These measurements indicate that a compression of 1.25 N is conservative enough to assure complete valve closure and restrict any downstream gravitational flow.

3.2. Pump actuator

The dependence of flow rate on actuation frequency and pump stroke phase was determined for the PDMS diffuser pumps. Two 25 μl capacity wells were punched out of the membrane, one at the inlet and the other at the outlet of the pump. The polystyrene supported membrane was laid flat on an optical breadboard. Fluid was allowed to fill the pump chambers by capillary action. When using water it was occasionally necessary to help the fluid along by applying a vacuum to the output end of the pump. The actuator block was suspended above, and precisely oriented over, the membrane with a three-axis micromanipulator. One micromanipulator controlled the vertical distance between the actuator block and the fluidics

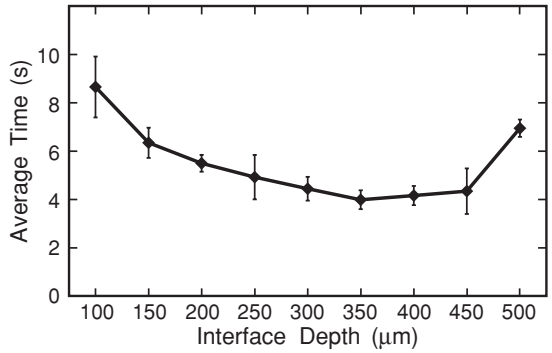

Figure 10. Pumping rate as a function of the pump plunger displacement, measured by the time required to pump 25 μl of water. A shorter time corresponds to a faster pumping rate.

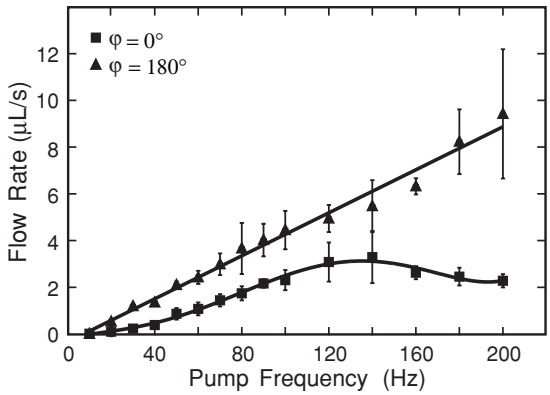

Figure 11. Water pumping rate as a function of actuator frequency for both in-phase and anti-phase actuation of the two pump plungers.

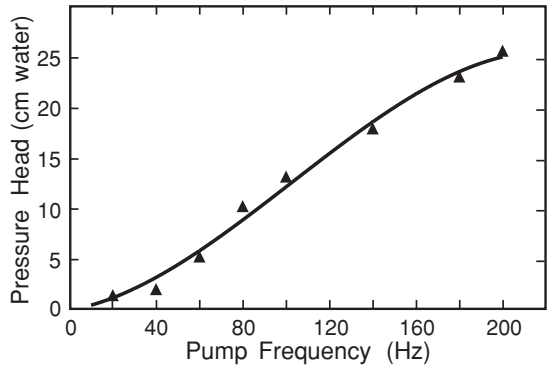

Figure 12. Pressure head generated by the pump as a function of the actuator frequency (anti-phase actuation).

membrane. The actuator frequency was selected with a sweep function generator and monitored on a digital oscilloscope.

Olsson *et al* [29] had previously noted that anti-phase pumping decreases the fluidic pulsations inherent to a diaphragm-based pump. Based on this knowledge, the pump was first tested in this configuration to determine what interface depth/compression distance between the pump actuator plunger and PDMS pump diaphragm would provide the optimal flow rate. The actuator-pump diaphragm distance was controlled by a micromanipulator. Compression depths between 50 μm and 500 μm were tried. For each repetition, the inlet well was filled with 25 μl of water. The elapsed time was noted at which the entire contents of the inlet well were emptied. As shown in figure 10, the highest flow rate (shortest evacuation time) was observed for a compression distance of 350 μm. This may seem large compared to the 125 μm height of the pump chambers. However, the distance also includes the compression, or 'give', of the silicone material at the point of contact with the pump actuator plungers during the inward deflection of the pump diaphragm.

Flow rate tests were also done comparing in-phase versus anti-phase actuation: in-phase actuation is when the actuators are compressing the diaphragms of the two PDMS pumps simultaneously and anti-phase actuation is when the diaphragm of one pump is being compressed while the second is being decompressed. Ten measurements were made for each decade of frequency from 10 to 100 Hz. Ten measurements were then made for every 20 Hz increment from 120 to 200 Hz. For each repetition the inlet well was filled with 25 μl of water, and the elapsed time measured for the entire contents of the inlet well to be emptied. The reported values in figure 11 reflect the average of the ten measurements made at each tested frequency. In-phase pumping ($\varphi = 0^\circ$) resulted in a nonlinear, and reduced, fluid throughput. Anti-phase pumping ($\varphi = 180^\circ$) produced a smooth fluid flow with the desired linear dependence between flow rate and pump frequency. Whereas in-phase pumping was limited to a maximum of 3 μl s^{-1} at 140 Hz, anti-phase pumping resulted in a rate of 4.3 μl s^{-1} at the median operating frequency of 100 Hz, and reached almost 10 μl s^{-1} at 200 Hz.

Anti-phase pumping was also used to assess the amount of head pressure against which the PDMS pump was capable of pumping. Water was pumped straight up a rigid tube from which the height of the water for each pump frequency measured between 10 Hz and 200 Hz. It was determined that the pump is capable of producing a pressure head difference of 25.6 cm (equivalent to ∼2.51 kPa) at a pump frequency of 200 Hz (figure 12).

Finally, flow rate tests were made using the buffer solution used in our DNA assays in order to examine the pump's ability to handle realistic assay reagents. In addition to containing 0.0125% w/v of SDS, the buffer solution also contained 2.81×10^8 beads ml^{-1} of 0.77 μm diameter magnetic microbeads (Seradyn SeraMag). Testing was done in a similar fashion to the water tests. The effect of the included detergent is immediately apparent: the average flow increases 1.6 times at comparable pumping frequencies because of the reduction of fluid surface tension caused by the detergent (figure 13). In addition, the pump performance is unaffected by the presence of microbeads in the solution.

3.3. Valve actuator

The performance of a valve cantilever was characterized with the same instrumentation set-up used during the PDMS compression test. To test the valve force, the probe of the load cell was brought into direct contact with the bead mounted at the tip of the cantilever beam. With power to the valve actuator turned on (open valve state), the load cell height was adjusted using the *Z*-axis micromanipulator such that the corresponding output from the load cell read 0 N. Removing power to the valve actuator (closed valve state) caused the

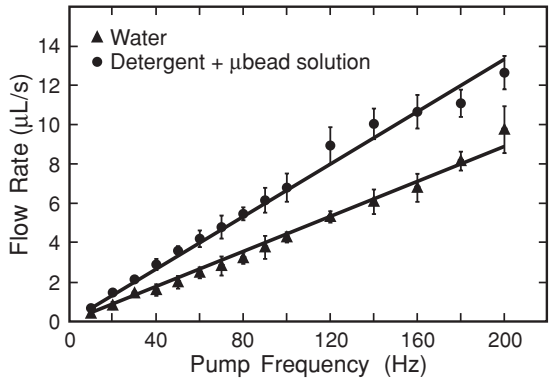

Figure 13. Flow rate as a function of actuator frequency (anti-phase actuation) for water versus a detergent solution containing microbeads (similar to what is used in a typical DNA assay).

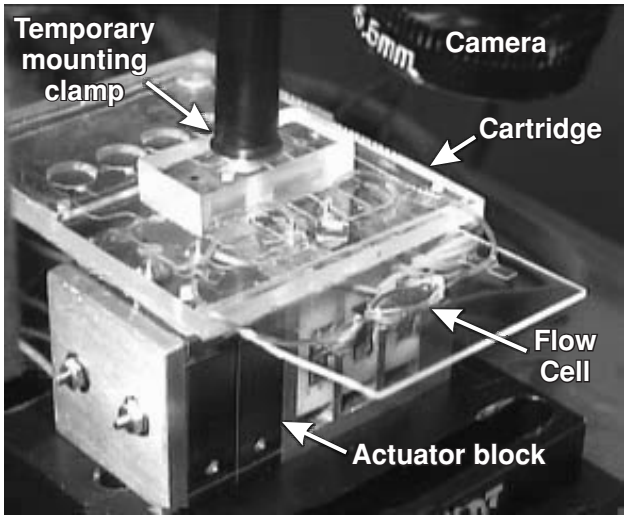

Figure 14. Photograph of the setup used to mechanically couple the cartridge to the actuator block assembly while on the workbench for study. In this case, a glass extender is attached to the cartridge in lieu of the chip carrier board, and a flow cell is mounted on a gold-coated silicon chip in lieu of a BARC sensor chip. This setup allows the complete fluidics operation to be optically monitored, including the biochemical assay.

cantilever to return to its resting position with 2.35 ± 0.01 N. This force is more than sufficient to close the pinch valves for both 10:1 and 5:1 PDMS mixtures. It takes approximately 0.8 s after removing power to the actuator to close the valve under a negative pressure of 37.92 kPa, and 2.7 s for the cantilever beam to traverse its entire range and return to its resting position. Finally, the total cantilever displacement was measured to be 406 μm using a linear variable differential transducer (LVDT).

4. Positive control assay demonstration

To demonstrate the complete functionality of the cartridge fluidics system, a bead capture assay was performed (figure 14). A gold-coated silicon chip was oxygen plasma cleaned and then arrayed with 200 μm diameter spots of biotinylated, single-stranded DNA (ssDNA) probes [17]. The chip was attached to a glass slide and a quartz flow cell

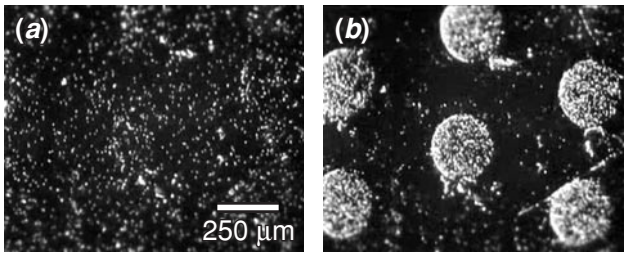

Figure 15. Video frames recorded through the flow cell during a positive assay where 2.8 μm diameter microbeads are captured onto a surface arrayed with 250 μm diameter spots of DNA. (*a*) The beginning of the assay showing early bead capture. (*b*) The end of the assay; each DNA spot is covered by microbeads, with relatively few beads bound elsewhere.

was then mounted on the silicon chip. Finally, the glass slide was secured to the cartridge and fluid interconnects between the cartridge and flow cell was made with TYGON microbore tubing. The assay demonstration was done on the optical breadboard so that the event could be captured on video. A metal post was screwed into the top center of the cartridge and used to secure the cartridge to the three-axis micromanipulator. The actuator block was carefully aligned beneath the cartridge to mate with the PDMS pump and pinch valves on the cartridge and secured to the optical breadboard. The cartridge was lowered toward the actuator block with the manipulator until contact was made at the correct compression distance. Throughout the assay demonstration, a pump actuation frequency of 100 Hz was used.

The cartridge fluidic channels and cell were primed with 1X SSC + 0.125% SDS buffer solution. Separate volumes of deionized water, 1X SSC + 0.125% SDS buffer solution, 5 mg ml^{-1} thiolated polyethylene glycol (PEG) solution, and 6.7×10^6 beads ml^{-1} of streptavidin-coated magnetic microbeads (M280 Dynabeads) in buffer solution were then placed in the individual wells of the cartridge. The pump was briefly turned on, allowing the buffer solution to flow through and purge any bubbles. Gold surface areas not covered with ssDNA probes were then coated with PEG by flowing the thiolated PEG solution over the chip for 30 s, stopping the flow for 5 min, and restarting the flow of PEG for another 30 s. Deposition of a PEG layer prevents non-specific binding of the magnetic microbeads to the gold surface [17]. After allowing the PEG solution to sit in the flow cell for a final 10 min, the surface was rinsed for 30 s with water. The flow cell was then filled with buffer solution that was allowed to remain in the cell for 1 min. Dynabeads functionalized with streptavidin were then introduced into the cell for a total duration of 12 min in the following intervals: 30 s bead flow, 3 min stopped flow (to allow beads to settle), 30 s bead flow, 1 min stopped flow, 30 s bead flow, 1 min stopped flow, 30 s bead flow, 3 min stopped flow. Finally, buffer was flowed through the cell for 2 min to remove non-specifically bound beads. Within the first 30 s of the bead flow, beads could already be seen being captured by binding between the biotinylated DNA probes immobilized on the substrate surface and the streptavidin on the beads. At the end of this successful assay, all arrayed spots were covered with a dense layer of beads with comparatively few beads bound non-specifically on the substrate between spots (figure 15).

Following the successful operation of the complete fluidics system on the optical breadboard, the actuator block was installed in the mechanical assembly (figure 5), so that the electrical and mechanical components are now all housed in a single case. All pump and valve operations are now being performed by simply inserting the cartridge through the opening in the case and running the control software. The performance of biochemical assays performed in this way will be discussed in a separate publication.

5. Summary

We have developed a hybrid fluidics platform for a chip-based biosensor system that combines high-performance microfluidics components with powerful, yet compact, millimeter-scale pump and valve actuators. The PDMS-based microfluidics components are included in a plastic cartridge that interfaces with a separate actuator block containing mechanically amplified piezoelectric pump actuators and SMA-activated cantilever valve actuators. All components can be fabricated from nonmagnetic components without the need for complex lithography or micromachining, and can be used with fluids containing micron-sized particulates. Careful pre- and post-fabrication engineering studies of the critical components ensured reliable operation of the completed system—the delivery of microliter volumes of fluid and the even dispersion of magnetic microbeads over the chip sensing elements. By taking a hybrid approach to the fluidics system, the biochemical assay benefits from the many advantages of microfluidics yet we avoid the complexity and unknown reliability of immature microactuator technologies.

Acknowledgments

C Tamanaha would like to thank the American Society for Engineering Education and the Naval Research Laboratory for the postdoctoral fellowship under which much of this work was made possible. Special thanks to R Edelstein for establishing the DNA probe assay conditions and P Sheehan for spotting chips with DNA probe samples. This work was supported in part by the US Defense Advanced Research Projects Agency and the US Office of Naval Research.

References

[1] Mitchell P 2001 *Nature Biotechnol.* **19** 717–21
[2] van Lintel H T G, van de Pol F C M and Bouwstra S 1988 *Sens. Actuators* **15** 153–67
[3] Shoji S, Nakagawa S and Esashi M 1990 *Sens. Actuators* **A21-A23** 189–92
[4] Mizoguchi H, Ando M, Mizuno T, Takagi T and Nakajima N 1992 *Proc. IEEE Micro Electro Mech. Syst. (MEMS'92) (Travemünde, Germany, February 4–7, 1992)* pp 31–6
[5] Gravesen P, Branebjerg J and Jensen O S 1993 *J. Micromech. Microeng.* **3** 168–82
[6] Sevick E M and Williams D R M 1994 *Macromolecules* **27** 5285–90
[7] Büstgens B, Bacher W, Menz W and Schomburg W K 1994 *Proc. IEEE Workshop on Micro Electro Mech. Syst. (MEMS'94) (Oiso, Japan, January 25–28, 1994)* pp 18–21
[8] Forster F K, Bardell R L, Afromowitz M A, Sharma N R and Blanchard A 1995 *Proc. ASME Fluids Engineering Division (San Francisco, CA, November 1995)* vol 234 pp 39–44
[9] Guo S, Nakamura T, Fukuda T and Oguro K 1996 *Proc. IEEE 7th Int. Symp. on Micro Machine and Human Science (MHS'96) (Nagoya, Japan, October 2–4, 1996)* pp 235–40
[10] Jun T K and Kim C J 1998 *J. Appl. Phys.* **83** 5658–64
[11] Böhm S, Olthuis W and Bergveld P 1999 *Sens. Actuators* A **77** 223–8
[12] Unger M A, Chou H-P, Thorsen T, Scherer A and Quake S R 2000 *Science* **288** 113–6
[13] Rife J C, Bell M I, Horwitz J S, Kabler M N, Auyeung R C Y and Kim W J 2000 *Sens. Actuators* A **86** 135–40
[14] Duffy D C, McDonald J C, Schueller O J A and Whitesides G M 1998 *Anal. Chem.* **70** 4974–84
[15] Whitesides G M and Stroock A D 2001 *Phys. Today* **54** 42–8
[16] Baselt D R, Lee G U, Natesan M, Metzger S W, Sheehan P E and Colton R J 1998 *Biosens. Bioelectron.* **13** 731–9
[17] Edelstein R L, Tamanaha C R, Sheehan P E, Miller M M, Baselt D R, Whitman L J and Colton R J 2000 *Biosens. Bioelectron.* **14** 805–13
[18] Alberts B, Bray D, Lewis J, Raff M, Roberts K and Watson J D 1994 *Molecular Biology of the Cell* (New York: Garland Publishing)
[19] Stege H, Roza L, Vink A A, Grewe M, Ruzicka T, Grether -Beck S and Krutmann J 2000 *Proc. Natl. Acad. Sci.* **97** 1790–5
[20] DeBusschere B D, Borkholder D A and Kovacs G T A 1998 *Technical Digest of the 1998 Solid-State Sensor and Actuator Workshop (Hilton Head Island, S.C., June 7–11, 1998)* pp 358–62
[21] Kumar A and Whitesides G M 1993 *Appl. Phys. Lett.* **63** 2002–4
[22] Delamarche E, Bernard A, Schmid H, Michel B and Biebuyck H 1997 *Science* **276** 779–81
[23] Zeringue H C, Glasgow I K, Beebe D J, Lyman J T and Wheeler M B 1999 *Proc. 21st Ann. Int. Conf. IEEE EMBS and 1999 Ann. Fall Meeting Biomed. Eng. Society (Atlanta, GA, October 13–16, 1999)* p 851
[24] Kuo A C M 1999 *Poly (dimethylsiloxane) Polymer Data Handbook* ed J E Mark (New York: Oxford University Press) pp 411–35
[25] Madou M J 1997 *Fundamentals of Microfabrication* (New York: CRC Press)
[26] Stemme E and Stemme G 1993 *Sens. Actuators* A **39** 159–67
[27] Instruction pamphlet *Toner Transfer System* (Clearwater: DynaArt Designs)
[28] Olsson A, Enoksson P, Stemme G and Stemme E 1997 *J. Microelectromech. Syst.* **6** 161–6
[29] Olsson A, Stemme G and Stemme E 1995 *Sens. Actuators* A **47** 549–56
[30] King T and Wei X 1996 *Robot. Auton. Syst.* **19** 189–97
[31] Smith S T, Badami V G, Dale J S and Xu Y 1997 *Rev. Sci. Instrum.* **68** 1474–83
[32] Gilbertson R G 1994 *Muscle Wires Project Book* (San Anselmo: Mondo-tronics, Inc.)